Title
Multiscale model of proton transport in perfluorosulfonic-acid membrane

Journal
ECS Transactions, 69(17)

ISSN
1938-6737

ISBN
9781607685395

Authors
Crothers, AR
Radke, CJ
Weber, AZ

Publication Date
2015

DOI
10.1149/06917.0731ecst

Peer reviewed

ECS Transactions, 69 (17) 731-742 (2015)
10.1149/06917.0731ecst ©The Electrochemical Society

Multiscale Model of Proton Transport in Perfluorosulfonic-Acid Membrane

Andrew R. Crothers[a,b], C. J. Radke[a,b], Adam Z. Weber[a]

[a]Lawrence Berkeley National Laboratory, 1 Cyclotron Rd, Berkeley, CA 94720
[b]Department of Chemical Engineering, University of California, Berkeley, CA 94720

Ionic conductivity in phase-separated polymer-electrolyte–fuel-cell membranes is limited by the multiple scales via which protons travel. The interactions of protons in the conducting pores determine the mobility at the nanoscale, while the tortuosity of the conductive phase dictates the macroscopic conductivity. Previous efforts to model transport in this multiscale network have relied on assumptions of the morphology. In this paper, direct imaging of a hydrated membrane is used to construct a realistic network through which transport occurs. Results indicate that pore-level proton conductivity is lower than the corresponding bulk-solution conductivity due to hydronium solvation at negative moieties of the polymer sidechains. Free protons in the pores diffuse at nearly bulk-like rates. The distribution of sizes of the hydrophilic transport domains leads to inhomogeneous transport pathways across the network.

Introduction

Ensuring rapid transport of protons in polymer electrolytes is an important challenge for improving fuel-cell performance. The most common type of polymer electrolyte is Nafion (from DuPont). Nafion is a perfluorinated sulfonic-acid (PFSA) ionomer, which is composed of a hydrophobic polytetrafluoroethylene backbone with perfluorovinyl ether side chains that terminate in a hydrophilic sulfonic-acid endgroup. The membrane is a random co-polymer that nanophase separates into backbone-rich hydrophobic and side-chain-rich hydrophilic phases (1). The spacing between these domains is on the order of 3 to 5 nm. During fuel-cell operation, water is sorbed into the hydrophilic regions and the ionomer swells. The phase-separated nature of the membrane allows proton transport through the interconnected hydrophilic-domain network. Proton transport increases slightly more than linearly with water content (2). Understanding proton transport through this network is important for developing design paradigms for new chemistries and optimizing overall device performance.

Transport in PFSA membranes occurs on multiple scales because protons are transported through a network that spans tens of micrometers or more but that consists of local hydrophilic regions with sizes on the order of nanometers. Pore-scale phenomena may alter proton transport from solution behavior due to interactions between the sulfonic-acid groups, water molecules, the hydrophobic backbone, side chains, and protons. Resistor-network models are appealing to address the multiple length scales due to low computational cost and a flexible framework that can incorporate both pore- and network-scale phenomena (3,4).

Resistor-network models were originally applied to model transport in porous media (3). Each pore is treated as a resistor with the resistance dependent on the size and geometry of the pore. The network of transport pathways through the porous medium is represented by a network of ideal resistors. Although a PFSA membrane is not a porous medium, resistor-network models have been adapted to PFSA membranes. These models have used effective-medium approximations (5–8) or modeled the network explicitly (9,10) to study ionic conductivity as a function of water content. These models incorporated pore-scale transport phenomena through empirical relationships that vary continuously as a function of pore-sizes (10), or treated pore transport as falling into a bimodal distribution of dry and wet pores with transport properties determined with phenomenological relationships (6) or molecular-dynamics simulations (9). Current models of PFSA membranes do not provide robust predictive capabilities because they rely on empirical relationships (6), scattering experiments (9,10), or porosimetry (8) for pore-size distributions, which provide only indirect evidence of the internal structure of the polymer membrane. Recent imaging of a hydrated Nafion PFSA film (11) creates the opportunity to overcome this limitation by extracting networks directly from images constructed from 3D-tomographic microscopy.

The goal of this paper is to construct a resistor network for proton transport in a PFSA membrane using 3D images of Nafion and to determine the effective macroscopic conductivity as a function of pore-scale connectivity. The pathways for transport are extracted via methods commonly used in research of porous media (12). The morphology of PFSA membranes is flexible and continuously changing at operating temperatures while the 3D-tomograph used to develop the network was taken under cryogenic conditions. Analysis of the extracted network is a representation of one configuration through which transport can occur at a given time point. The deviations from bulk-solution conductivity in the pores due to immobile protons and electrostatic frictional forces are examined.

Network Extraction

Binarization

Cryogenic transmission-electron microscopy was used to construct a 3D image of a cast, liquid-water-equilibrated Nafion film (11). Resultant images were analyzed using Avizo 8 Fire software. The voxel size was 0.224 nm. To differentiate the hydrophilic domains in which transport occurs from the hydrophobic domains, the phases boundaries were defined by thresholding the greyscale images, which resulted in 0.57 volume fraction of hydrophilic phase, which agrees with experimental measurements, and was shown to result in Fourier-space agreement with small-angle X-ray scattering experiments (11). To improve differentiation of domains for network-extraction algorithms, a median filter was applied to the greyscale image. The filtering process eliminated small features of hydrophilic and hydrophobic domains. These small domains were assumed to be noise artifacts or, if genuine, to exhibit negligible impact on the transport pathways.

Skeletonization

The medial centerline of interconnected transport pathways of hydrophilic domains (the network skeleton) was extracted from a 90x90x56 nm rectangular prism. The dimensions of a segment are defined by the length, thickness and width. The distance between each

connected node is defined as the length of a segment. The distance from the center of a hydrophilic phase to the nearest hydrophobic-phase boundary along a segment lines is defined as half the thickness of that segment. The width of a segment is defined as the distance between hydrophobic phases perpendicular to the length and thickness direction. The cross-section of the segment is defined as the width by the thickness. This results in greater than 106,000 segments in the network, where each one represents a resistor in the network.

Theory

Segment Conductivity

To determine the effective macroscopic conductivity of the network, the conductivity of each nanoscale segment in the network must be established. To understand how different types of transport resistances impact the effective network conductivity, three methods were used to determine the segment conductivity: (1) setting the conductivity to that of protons in a solution, (2) setting the conductivity to that of protons in solution but accounting for protons that are immobile in the first solvation shell of negatively charged sulfonic acid moieties of the polymer, and (3) determining the conductivity by accounting for immobile protons as well as frictional forces between free protons and sulfonic acid groups. Details of each method are discussed below.

Scenario 1: Solution-Like Conductivity. To determine the impact of tortuosity and develop an upper limit of conductivity for the network, the conductivities for each segment of the network were set as an estimate of the conductivity of H^+ in a bulk aqueous solution. Limiting molar conductivity of a given ion pair in a dilute solution is given as

$$\Lambda^0 = \nu_A \lambda_A^0 + \nu_B \lambda_B^0 \qquad [1]$$

where ν_i is the stoichiometric coefficient of ion i in the solution with limiting molar ionic conductivity of λ_i^0. Values of λ_i^0 in dilute solution were determined experimentally (13). The molar conductivity is equal to the ionic conductivity divided by the concentration of the ions in solution. The conductivity of protons in a bulk aqueous solution at the concentration found in the pores of a PFSA membrane were determined via the equation

$$\kappa = \frac{\lambda_{H^+}^0}{\hat{V}_W n} \qquad [2]$$

where κ is the conductivity, $\lambda_{H^+}^0$ is the limiting molar conductivity of protons (equal to 349.8 S cm^2 mol^{-1} (13)), $\hat{V}_W$ is the molar volume of water, and n is the number of moles of water per mole of sulfonic acid groups in the polymer (22 in a liquid-water saturated membrane (11)). Because the negatively charged sulfonic acid groups are functionalized to the polymer, protons are the only ion that participates in conduction. Using this methodology, a value of 0.87 S/cm was determined as the conductivity of protons in a solution at the same concentration as that found in the membrane, and the conductivity of each segment in the network was set to this value in this scenario.

Scenario 2: Solution-Like Conductivity with Immobile Protons. In the second scenario, the impact of protons that are immobile because they are solvated or bound to sulfonic acid groups is examined. How to quantify the fraction of protons that are mobile and participate in conduction is not straightforward (14–19). Estimates of the fraction of protons dissociated from the sulfonic-acid groups in hydrated PFSA ionomer range from 2 to 100% (1,14,20). Even for protons that are dissociated, many exist in the first hydration shell with low mobility. Estimates of the fraction of protons that exist in the first hydration shell in a hydrated membrane range from ~40% (15–17) to over 90% (18,19). As the Nafion film studied here had a high water content because it was equilibrated in liquid water, the fraction of condensed protons is assumed to be negligible. The fraction of protons that remain immobile in the first hydration shell was chosen to be 40% based on molecular-dynamics simulation of liquid-equilibrated Nafion by Devanathan et al. (16). The conductivity of free protons was set to the solution-level conductivity discussed in the preceding scenario. The pore conductivity was therefore 60% of the conductivity in determined in Scenario 1, 0.52 S/cm.

Scenario 3: Conductivity Accounting for Immobile Protons and Additional Frictional Forces. In the third scenario, the impact of frictional interactions on protons outside the first solvation shell were determined using a statistical-mechanics model for proton transport in a cylindrical ionomer pore developed by Paul et al. (21–23). This model was used to calculate the diffusion coefficient of a hydronium ion from the friction coefficient due to interactions with the water molecules and sulfonic-acid groups. The solvent-hydronium friction coefficient was taken as that measured for bulk water following (24) to incorporate bulk-like Grotthuss hopping proton-transport mechanism. This approach to incorporating proton hopping is somewhat artificial as the mechanism for proton hopping is complex; it is unclear how hopping and vehicular transport are correlated (25) or how hopping is altered in the pores of PFSA membranes. The friction coefficient of the hydronium ion due to sulfonic-acid sites acting through solvent mediation was shown to dominate in most cases, and was the only additional friction coefficient beyond direct friction between the solvent and hydronium ions that was incorporated into this formulation of the model. The diffusion coefficient as a function of distance across the pore can be determined and used to calculate the conductivity of a pore as a function of thickness of the pore by integrating the Nernst-Einstein relationship across the thickness direction,

$$\kappa_{seg}(a) = \frac{F^2}{RTa}\int_0^a D(y)c(y)dy \qquad [3]$$

where a is the thickness of a segment, y is the distance from the pore wall, F is the Faraday constant, R is the gas constant, T is the temperature, D is the diffusivity of hydronium ions, and c is the concentration of hydronium ions. In using this formulation, we assume that the Nernst-Einstein relationship is valid at the hydronium ion concentrations in the membrane (2.5 M).

The concentration of protons in the hydrophilic pores is not agreed upon (26) and a method for calculating charge densities are not specifically endorsed in the statistical-mechanics model that is used in this study (22). For simplicity, the location of protons is assigned to a bimodal distribution where the population of protons in the first solvation shell of sulfonic acid groups is located at the walls of the pores with a diffusivity of zero while free protons are evenly spread across the volume of the pore with a diffusivity as

calculated at the point along the cross-section of the pore farthest from the sulfonic acid groups. The segment conductivity is then

$$\kappa_{seg}(a) = \frac{F^2}{RTV_w n_{free}} D_{max}(a) \quad [4]$$

where D_{max} is the diffusivity at the point farthest from a the sulfonic acid groups and n_{free} is the number of water molecules per sulfonic acid group not in the first solvation shell. The fraction of protons in the first solvation shell was set to 40% based on molecular-dynamics calculations (16). This method underestimates the diffusivity of protons in the first solvation shell, which in reality has a nonzero value, and overestimates the diffusivity of protons that are free, which is less than the maximum diffusivity in the pore for most protons.

The statistical-mechanics model used to calculate diffusivity is formulated for a cylindrical pore (22). To apply the results of the diffusivity model, which uses a cylindrical geometry, to the slit geometry of the system analyzed here, pore thickness is substituted for pore radius in determining the diffusivity at the point farthest from the sulfonic acid groups. This substitution is justified on the basis that proton transport will have the highest diffusivity at the point in the pore farthest from the negatively-charged sulfonic-acid groups. At relatively low surface-charge densities and in fully hydrated membranes, sulfonic-acid groups do not fall directly across the channel width but are offset (16). Therefore, the distance at which the proton diffusion rate is the highest is the thickness of the segment in the flat, slit domain-structure found in the tomograph while the point farthest from the sulfonic acid groups in the cylindrical geometry of the model is the radius. The diffusion coefficient was therefore determined in the center of a liquid-equilibrated Nafion pore with a varying radius while keeping the volume, surface charge density, and ratio of water molecules to sulfonic-acid groups constant at 22. The conductivity of pores varied with pore thickness in this scenario with a mean of 0.35 S/cm.

Network Conductivity

At steady state, the current, as determined using Ohm's law, through each node in the network is equal to the net of current in every segment leading to the node. A current balance on node *i* that is connected to *N* other nodes is thus

$$0 = \sum_{k=1}^{N} (V_k - V_i) \frac{\kappa_{seg,ik} A_{ik}}{l_{ik}} \quad [5]$$

where V is the potential at a node, the subscript k denotes a node connected to node i, A_{ik} is the cross-sectional area of the segment connecting nodes k and i calculated as the thickness of the segment multiplied by the width of the segment, and l_{ik} is the length of the segment. This procedure results in a matrix of equations for the current at each node. By setting the voltage at the boundaries nodes and inverting the matrix, the current and effective conductivity of the network is determined. The software OpenPNM was used to run the simulations (27).

Results and Discussion

Network

Figure 1 shows that branching occurs at most nodes as indicated by a coordination number of three. The distribution of segment lengths are skewed to the right with a broad peak around a median of 2.0 nm, as shown in Figure 2(a). The hydrophilic domains are locally flat with a width of 2.5 nm (11). The thickness of a network segment was calculated as twice the mean distance from the centerline of a hydrophilic segment to the hydrophobic phase. The distribution of the thicknesses of the segments has a broad peak around a median of 0.78 nm and is also skewed right, as shown in Figure 2(b). The absence of data below 0.22 nm is due to the limit of imaging resolution. As the diameter of a water molecule is approximately 0.3 nm, the lower end of the thickness measurements has limited physical meaning. The thicknesses and lengths of the segments followed a log-normal distribution with a probability distribution function, *f*, given by

$$f = \frac{1}{x\sigma\sqrt{2\pi}} e^{-\frac{(\ln x-\mu)^2}{2\sigma^2}} \quad [6]$$

where x is the independent variable of the distribution and σ and μ are the mean and standard deviation of the natural logarithm of the distribution.

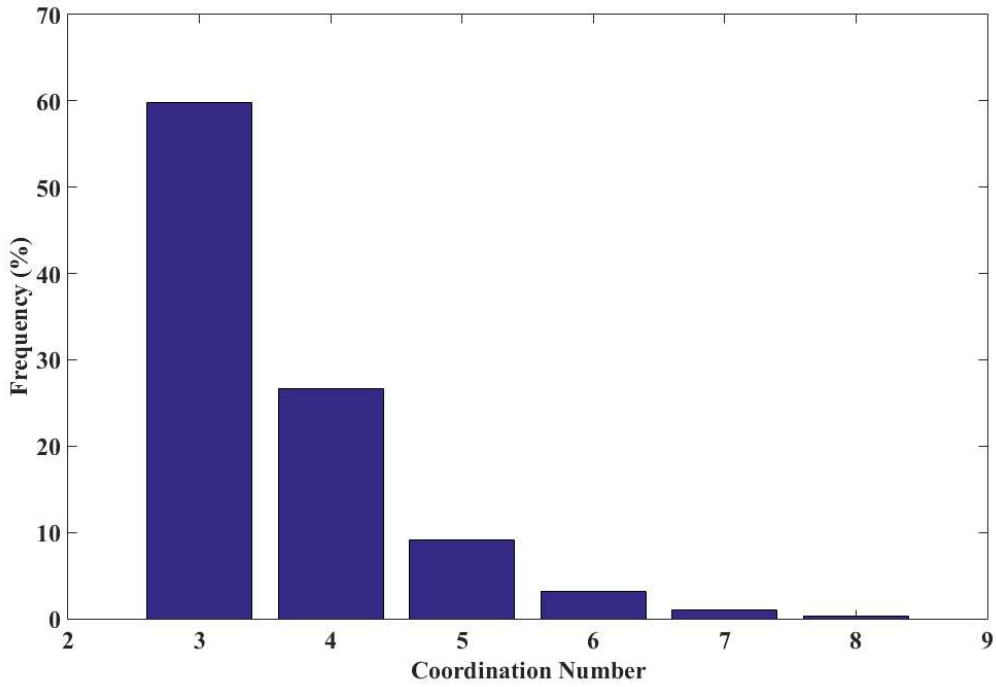

Figure 1. Histogram of the number of connections from each node in the network

(a)

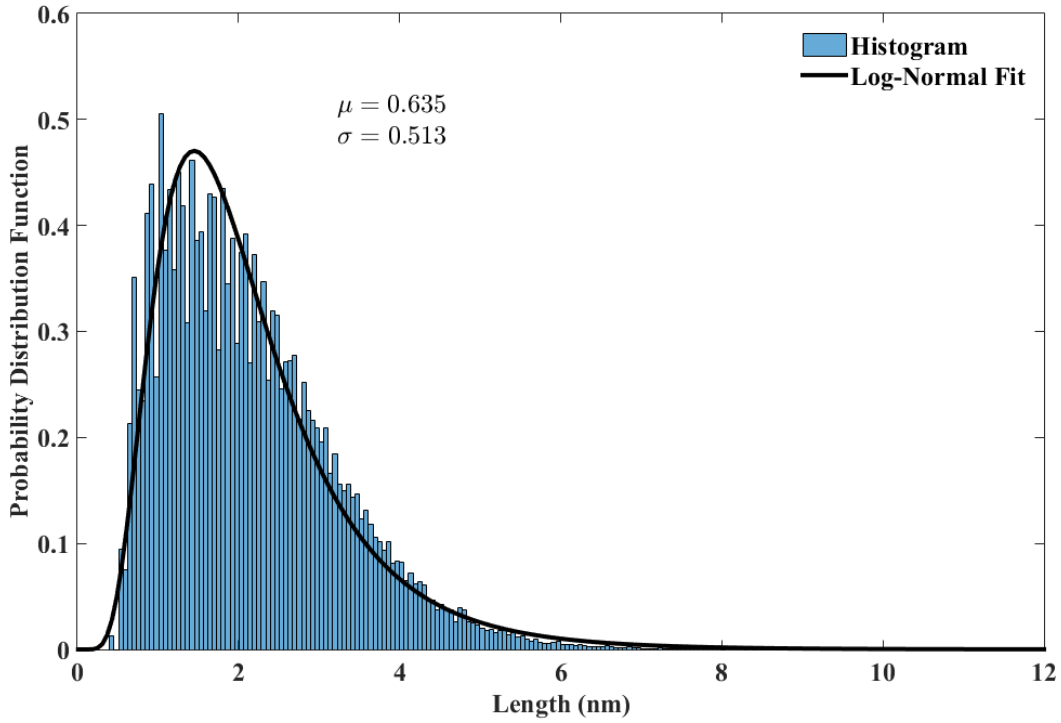

(b)

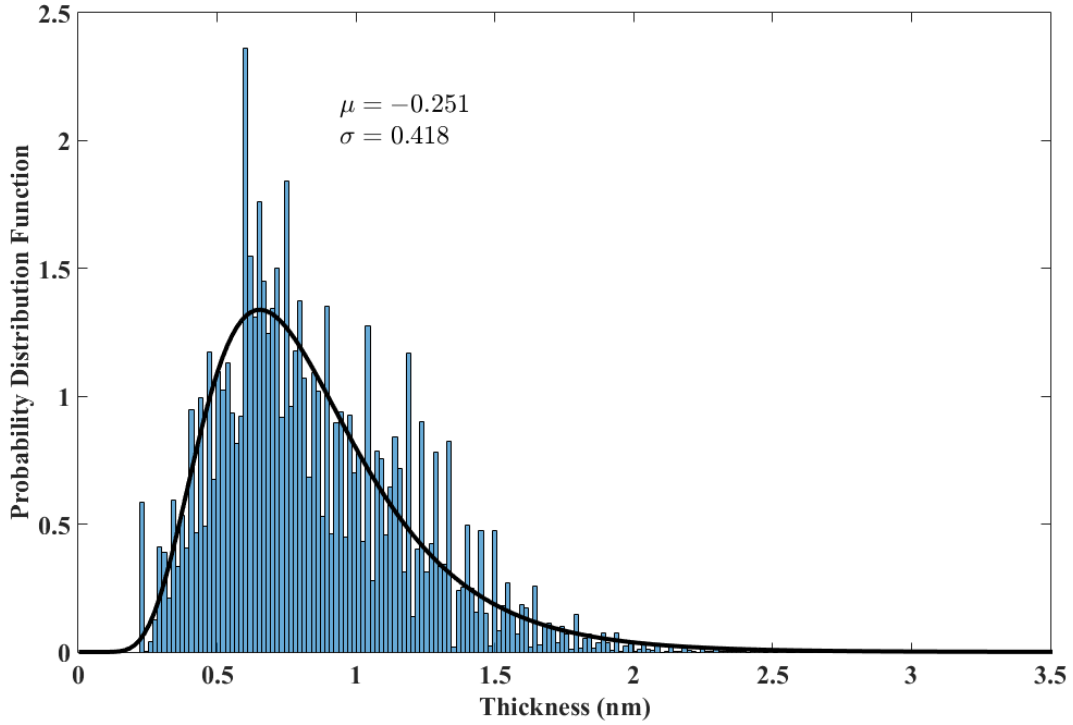

Figure 2. Statistics of network segments and log-normal fits to the distributions where (a) is a histogram of the lengths of the segments and (b) is a histogram of twice the mean distance from the centerline of a hydrophilic network segment to the hydrophobic phase.

These results show that hydrated Nafion consists of a hydrophilic network of short, branching connections that mediate transport through the membrane. This structure is consistent with X-ray and neutron scattering, which show the morphology of Nafion to be locally flat hydrophilic domains with a thickness on order of 1 nm separated by polymer fibrils with hydrophobic cores (28–31). The domain spacing of Nafion measured from scattering (32) and visual inspection of the tomograph is approximately 5 nm, which is two-and-a-half times as large as the distance between node points on the network. The nodes are not large pore-bodies that constitute the center of hydrophilic domains but are points where splitting of hydrophilic pathways occurs. In the median segment connecting two nodes on the network, there are approximately 107 water molecules and 5 sulfonic acid sites.

Effective Conductivity

The effective network conductivity of the three methods used to calculate segment conductivity are shown in Figure 3. The Scenario 1 network conductivity at 0.17 S/cm is higher than experimental measurements of 0.11 S/cm, while Scenario 2 and 3 at 0.10 S/cm and 0.053 S/cm respectively, are lower.

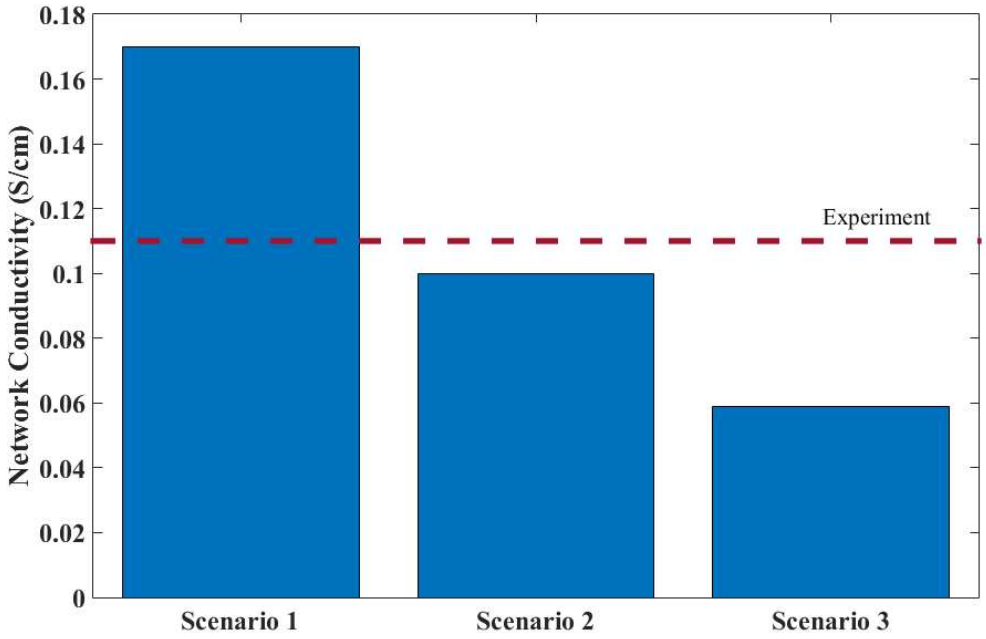

Figure 3. Comparison of the effective conductivity of three methods for calculating the segmental conductivity. In Scenario 1 all protons diffuse at a rate as if in an aqueous solution. In Scenario 2 a fraction of protons that are immobile in the first solvation shell of a sulfonic acid group while free proton diffuse at a rate as if in an aqueous solution. In Scenario 3, free protons diffuse at a reduced rate from an aqueous solution due to interactions between sulfonic acid groups and protons. The dashed line is the conductivity of the membrane from experiments (7).

The effective conductivity from Scenario 1 shows the degree to which the tortuosity of the network reduces conductivity. The tortuosity, τ, of the network was determined to be 2.9 as defined by

$$\tau = \phi \frac{\kappa_{solution}}{\kappa_{network}} \quad [7]$$

where ϕ is the volume fraction of the hydrophilic phase and κ is the conductivity.

There are a plethora of other factors that can influence proton transport through PFSA membranes beyond the simple structure of the network that is accounted for in Scenario 1. If the molar conductivity decreases from the infinite-dilution limit at high ionic concentrations, as is the case for most aqueous electrolyte solutions, the conductivity will be lower. If not all the protons are dissociated from the sulfonic-acid sites, the conductivity will be lower as fewer ions will be mobile. If there are additional frictional forces on proton transport through the membrane that are not present in solution, such as interactions with sulfonic-acid groups, the conductivity of the network will be lower as the dissociated protons will have hindered mobility. Frictional forces may depend on water content, distribution of acid sites, mobility of side-chains, and relaxation rates of the polymer-backbone to name a few factors (20,15,21,25).

Scenarios 2 and 3 attempt to account for some of these additional factors. Scenario 2 takes into account that not all protons are completely mobile. The results of this scenario are close to experiments indicating that free protons diffusive relatively rapidly in the hydrophilic domains (33).

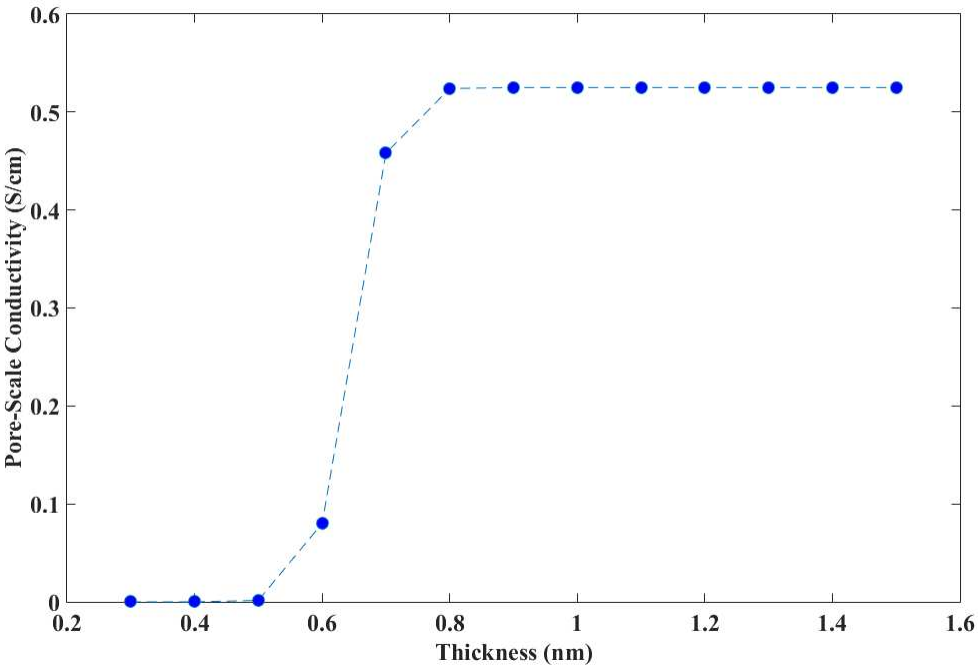

Figure 4. Pore conductivity as a function of domain thickness as calculated from the statistical-mechanics model for a cylindrical channel and the Nernst-Einstein relationship. Points are calculations while the dotted line guides the eye.

Scenario 3 provides insight into the degree to which interactions between free protons and negatively charged sulfonic acid groups reduce conductivity. The dependence between conductivity and segment thickness, in Figure 4, shows that the conductivity is lower in smaller pores but increases drastically for pores that are thicker than 0.6 nm and levels out beyond 0.8 nm to a solution rate of conductivity adjusted for the number of protons

immobile in the first hydration shell. As the distribution of segment thicknesses lies at 0.7 nm, the sharp increase in conductivity beyond 0.6 nm thickness means that conductivity is very sensitive to small shifts in the distribution of thicknesses.

The effective network conductivity of Scenario 3 resulted in an effective conductivity of the network smaller than experimental measurements. This error is likely due to differences in geometry between the statistical-mechanics model and the system modeled here. There may also be additional transport pathways that are not accounted for in this models such as hopping along hydrogen-bond networks in confined channels (34) or surface hopping between the first hydration shells of sulfonic-acid sites (35).

Pore-scale simulations have been used to gain an understanding of conductivity nanoscopically (18), but these methods do not directly provide insight into transport at the network-scale. Network simulations capture details of mesoscale transport-pathways. Figure 5 shows a representation of the network. Lines in the figure are segments of the network and the points where lines connect are nodes. Segments are colored based on the average electrostatic potential of the nodes connected by a segment while segments through which large currents pass are colored black (see figure title for details). If the membrane were treated as a homogenous medium, isopotential lines would be straight, vertical lines. Figure 5 shows that the medium is not homogenous, but has small non-uniformities existing across the network making isopotential lines (lines following a constant color) circuitous. There are dominant pathways in the network, as indicated by segments colored black, but these pathways do not stretch across the entire network. There are large regions through which little current passes.

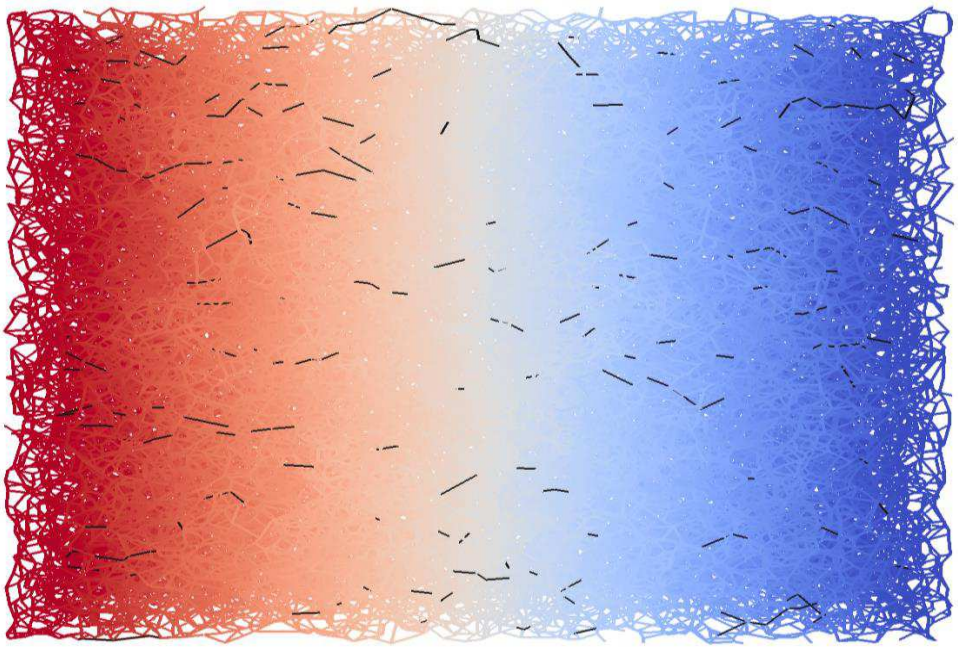

Figure 5. Proton transport in a 2D slice of the Nafion network. The lines in the figure are segments of the network connecting nodes. Segments are colored to show potential drop from high potential (red) to low (blue). Segments colored black are those with a current flux one standard deviation above the average.

Summary

A proton resistor network was extracted and determined from direct imaging of a PFSA ionomer membrane. The segments connecting nodes of the network were shown to be thin, with a median thickness of 0.76 nm. The upper limit of conductivity for the model was found to be 55% higher than experimental measurements by setting the conductivity of individual segments to the molar conductivity of protons in aqueous solution. Accounting for immobile protons and frictional forces inside the membrane using a statistical-mechanics-based model predicted an effective membrane conductivity of 0.059 S/cm. Results show that the transport network across the network is heterogeneous and there are regions of low conductivity in the membrane. This work demonstrates a methodology for how network models of ion-conducting membranes can bridge molecular level details and bulk properties. Considering the high degree of uncertainty in pore-scale interactions and morphology, the relatively close agreement between this simulation and experimental data provides an impetus for further investigation using resistor-network models.

Acknowledgements

This work was funded by the Assistant Secretary for Energy Efficiency and Renewable Energy, Fuel Cell Technologies Office, of the U. S. Department of Energy under contract number DE-AC02-05CH11231 and by a National Science Foundation Graduate Research Fellowship under Grant No. DGE 1106400. The authors thank Stephen Paddison for discussions on his statistical-mechanics model and Frances Allen for discussions on 3D cryo TEM image processing.

References

1. K. A. Mauritz and R. B. Moore, *Chem. Rev.*, **104**, 4535–4586 (2004).
2. M. A. Hickner and B. S. Pivovar, *Fuel Cells*, **5**, 213–229 (2005).
3. M. Sahimi, in *Flow and Transport in Porous Media and Fractured Rock*,, p. 179–211, Wiley-VCH Verlag GmbH & Co. KGaA (2011)
4. J. Bear, *Dynamics of fluids in porous media*, p. 1, Dover, New York, (1988)
5. S. Kirkpatrick, *Rev. Mod. Phys.*, **45**, 574–588 (1973).
6. M. Eikerling, A. A. Kornyshev, and U. Stimming, *J. Phys. Chem. B*, **101**, 10807–10820 (1997).
7. A. Z. Weber and J. Newman, *J. Electrochem. Soc.*, **151**, A311–A325 (2004).
8. P. Costamagna, S. Grosso, and R. Di Felice, *J. Power Sources*, **178**, 537–546 (2008).
9. G. S. Hwang et al., *Polymer*, **52**, 2584–2593 (2011).
10. J. T. Gostick and A. Z. Weber, *Electrochim. Acta*
11. F. I. Allen et al., *ACS Macro Lett.*, **4**, 1–5 (2015).
12. W. B. Lindquist, A. Venkatarangan, J. Dunsmuir, and T. Wong, *J. Geophys. Res. Solid Earth*, **105**, 21509–21527 (2000).
13. C. G. Zoski, *Handbook of Electrochemistry*, p. 935, Elsevier, (2006).
14. K. M. Beers, D. T. Hallinan, X. Wang, J. A. Pople, and N. P. Balsara, *Macromolecules*, **44**, 8866–8870 (2011).
15. S. Feng and G. A. Voth, *J. Phys. Chem. B*, **115**, 5903–5912 (2011).

16. R. Devanathan, A. Venkatnathan, and M. Dupuis, *J. Phys. Chem. B*, **111**, 8069–8079 (2007).
17. I. H. Hristov, S. J. Paddison, and R. Paul, *J. Phys. Chem. B*, **112**, 2937–2949 (2008).
18. S. Liu, J. Savage, and G. A. Voth, *J. Phys. Chem. C*, **119**, 1753–1762 (2015).
19. P. Commer, A. G. Cherstvy, E. Spohr, and A. A. Kornyshev, *Fuel Cells*, **2**, 127–136 (2002).
20. J. K. Clark II and S. J. Paddison, *Electrochim. Acta*, **101**, 279–292 (2013).
21. S. J. Paddison, R. Paul, and T. A. Zawodzinski, *J. Electrochem. Soc.*, **147**, 617–626 (2000).
22. R. Paul and S. J. Paddison, *J. Chem. Phys.*, **123**, 224704 (2005).
23. R. Paul and S. J. Paddison, *J. Phys. Chem. B*, **108**, 13231–13241 (2004).
24. S. J. Paddison, R. Paul, and K.-D. Kreuer, *Phys. Chem. Chem. Phys.*, **4**, 1151–1157 (2002).
25. M. K. Petersen and G. A. Voth, *J. Phys. Chem. B*, **110**, 18594–18600 (2006).
26. K.-D. Kreuer, S. J. Paddison, E. Spohr, and M. Schuster, *Chem. Rev.*, **104**, 4637–4678 (2004).
27. A. Putz et al., *ECS Trans.*, **58**, 79–86 (2013).
28. K.-D. Kreuer and G. Portale, *Adv. Funct. Mater.*, **23**, 5390–5397 (2013).
29. H.-G. Haubold, T. Vad, H. Jungbluth, and P. Hiller, *Electrochim. Acta*, **46**, 1559–1563 (2001).
30. L. Rubatat, A. L. Rollet, G. Gebel, and O. Diat, *Macromolecules*, **35**, 4050–4055 (2002).
31. L. Rubatat, G. Gebel, and O. Diat, *Macromolecules*, **37**, 7772–7783 (2004).
32. A. Kusoglu, S. Savagatrup, K. T. Clark, and A. Z. Weber, *Macromolecules*, **45**, 7467–7476 (2012).
33. J.-C. Perrin, S. Lyonnard, and F. Volino, *J. Phys. Chem. C*, **111**, 3393–3404 (2007).
34. C. Dellago, M. M. Naor, and G. Hummer, *Phys. Rev. Lett.*, **90**, 105902 (2003).
35. S. Feng, J. Savage, and G. A. Voth, *J. Phys. Chem. C*, **116**, 19104–19116 (2012).